




## RESEARCH ARTICLE

# White matter hyperintensities induce distal deficits in the connected fibers

Yanpeng Liu<sup>1</sup>  | Yiwei Xia<sup>2</sup> | Xiaoxiao Wang<sup>1</sup>  | Yanming Wang<sup>1</sup> | Du Zhang<sup>1</sup> | Benedictor Alexander Nguchu<sup>1</sup> | Jiajie He<sup>1</sup> | Yi Wang<sup>2</sup> | Lumeng Yang<sup>2</sup> | Yiqing Wang<sup>2</sup> | Yunqing Ying<sup>2</sup> | Xiaoni Liang<sup>3</sup> | Qianhua Zhao<sup>3</sup> | Jianjun Wu<sup>2,4</sup> | Zonghui Liang<sup>5</sup> | Ding Ding<sup>3</sup> | Qiang Dong<sup>2</sup> | Bensheng Qiu<sup>1</sup> | Xin Cheng<sup>2</sup> | Jia-Hong Gao<sup>1,6,7</sup> 

<sup>1</sup>Hefei National Lab for Physical Sciences at the Microscale and the Centers for Biomedical Engineering, University of Science and Technology of China, Hefei, China

<sup>2</sup>Department of Neurology, National Clinical Research Centre for Aging and Medicine, Huashan Hospital, State Key Laboratory of Medical Neurobiology, Fudan University, Shanghai, China

<sup>3</sup>Institute of Neurology, National Clinical Research Centre for Aging and Medicine, Huashan Hospital, Fudan University, Shanghai, China

<sup>4</sup>Department of Neurology, Jing'an District Center Hospital, Shanghai, China

<sup>5</sup>Department of Radiology, Jing'an District Center Hospital, Shanghai, China

<sup>6</sup>Center for MRI Research and Beijing City Key Lab for Medical Physics and Engineering, Peking University, Beijing, China

<sup>7</sup>McGovern Institute for Brain Research, Peking University, Beijing, China

## Correspondence

Jia-Hong Gao, Center for MRI Research and Beijing City Key Lab for Medical Physics and Engineering, Peking University, Beijing, China.  
Email: chengxin@pku.edu.cn

Xin Cheng, Department of Neurology, National Clinical Research Centre for Aging and Medicine, Huashan Hospital, State Key Laboratory of Medical Neurobiology, Fudan University, Shanghai, China.  
Email: chengxin@fudan.edu.cn

Bensheng Qiu, Hefei National Lab for Physical Sciences at the Microscale and the Centers for Biomedical Engineering, University of Science and Technology of China, Hefei, China.  
Email: bqiu@ustc.edu.cn

## Funding information

National Key R&D Program of China, Grant/Award Numbers: 2016YFC1300503, 2017YFC1308201; National Natural Science Foundation of China, Grant/Award Numbers: 21876041, 81701665, 81971123; Shanghai Municipal Science and Technology Major Project, Grant/Award Number: No.2018SHZDZX01

## Abstract

White matter hyperintensities (WMH) are common in elderly individuals and cause brain network deficits. However, it is still unclear how the global brain network is affected by the focal WMH. We aimed to investigate the diffusion of WMH-related deficits along the connecting white matters (WM). Brain magnetic resonance imaging data and neuropsychological evaluations of 174 participants (aged  $74 \pm 5$  years) were collected and analyzed. For each participant, WMH lesions were segmented using a deep learning method, and 18 major WM tracts were reconstructed using automated quantitative tractography. The diffusion characteristics of distal WM tracts (with the WMH penumbra excluded) were calculated. Multivariable linear regression analysis was performed. We found that a high burden of tract-specific WMH was related to worse diffusion characteristics of distal WM tracts in a wide range of WM tracts, including the forceps major (FMA), forceps minor (FMI), anterior thalamic radiation (ATR), cingulum cingulate gyrus (CCG), corticospinal tract (CST), inferior longitudinal fasciculus (ILF), superior longitudinal fasciculus-parietal (SLFP), superior longitudinal fasciculus-temporal (SLFT), and uncinate fasciculus (UNC). Furthermore, a higher mean diffusivity (MD) of distal tracts was linked to worse attention and executive function in the FMI, right CCG, left ILF, SLFP, SLFT, and UNC. The effect of WMH on the microstructural integrity of WM

Yanpeng Liu, Yiwei Xia, and Xiaoxiao Wang contributed equally to this work.

This is an open access article under the terms of the Creative Commons Attribution-NonCommercial-NoDerivs License, which permits use and distribution in any medium, provided the original work is properly cited, the use is non-commercial and no modifications or adaptations are made.

© 2021 The Authors. *Human Brain Mapping* published by Wiley Periodicals LLC.

tracts may propagate along tracts to distal regions beyond the penumbra and might eventually affect attention and executive function.

#### KEYWORDS

cognition, diffusion tensor imaging, microstructural integrity, tractography, white matter hyperintensities

## 1 | INTRODUCTION

White matter hyperintensities (WMH), typical radiological markers of age-related cerebral small vessel disease (CSVD), are commonly observed in T<sub>2</sub>-weighted or fluid-attenuated inversion recovery (FLAIR) brain MRI images of elderly individuals (DeCarli et al., 2005; Wardlaw et al., 2013). The global WMH burden has been found to be associated with whole-brain atrophy, brain structural network efficiency, and cognitive decline (Banerjee et al., 2018; Maniega et al., 2015; Wardlaw, Smith, & Dichgans, 2019).

Studies have suggested that WMH may represent a wide range of degenerations, including demyelination, axonal loss, gliosis (Wardlaw et al., 2019) and impaired blood-brain barrier (BBB) (Black, Gao, & Bilbao, 2009). The deficits may intrude into the penumbra, normal-appearing white matter (NAWM) nearby, and affect the white matter (WM) infrastructure (Maillard et al., 2014) and cerebral blood flow (Promjunyakul et al., 2016). Moreover, the degenerative penumbra is larger in WMH-intersecting WM tracts than in nearby WMH-nonintersecting tracts (Munoz Maniega et al., 2019; Reginold et al., 2016; Reginold et al., 2018), suggesting that degenerations propagate along WM tracts. Thus, we seek to investigate whether WMH-related defects propagate to remote areas.

Diffusion tensor imaging (DTI) has provided a noninvasive approach to investigate early changes in WM microstructure (Alexander, Lee, Lazar, & Field, 2007). Tractography methods have been proposed and provide new insight into brain connectivity structure (Schilling et al., 2019). In the present study, automated quantitative tractography was used to reconstruct the major WM fiber tracts, and the diffusion characteristics (fractional anisotropy, FA; mean diffusivity, MD) were extracted. We attempted to investigate the relationship between tract-specific WMH burden and microstructural integrity of the distal tracts in community-dwelling elderly individuals. In addition, we evaluated the impact of the impaired distal tracts on cognitive impairment. We hypothesized that the effect of WMH on the microstructural integrity of WM tracts might propagate along tracts to distal regions beyond the penumbra.

## 2 | MATERIALS AND METHODS

### 2.1 | Study population

This study is part of the Shanghai Aging Study (SAS), which prospectively investigates the prevalence, incidence and risk factors for

cognitive impairment among elderly residents in the Jing'an Temple Community, an urban community of Shanghai, China. The detailed protocols for the study have been previously reported (Ding et al., 2014). The protocol of this SAS study was approved by the Institutional Review Board of Fudan University. The signed consent form was provided by each participant. From 2016 to 2018, a total of 262 eligible individuals were invited by telephone to undergo brain structural and diffusion MRI. The inclusion criteria were as follows: (a) age over 65 years; (b) residence in the Jing'an Temple Community. Participants were excluded if they had any of the following characteristics: (a) cerebral large vessel stenosis (>50%); (b) hydrocephalus or brain tumors; (c) MRI contraindications; (d) refusal or inability to complete the examination. Of the 262 recruited subjects, 71 refused to participate, and the remaining 191 participated in this study. In addition, 17 of the participants were excluded (12 for incomplete and mismatched images and 5 for poor image quality), resulting in 174 qualified participants.

### 2.2 | Vascular risk factors and medication use

Demographic characteristics, vascular risk factors, and medication use were collected via an interviewer-administered questionnaire, and were further confirmed in the patient history, these features comprised age; sex; years of education; body mass index; current smoking status; hypertension; diabetes; hyperlipidemia; cardiogenic disease (atrial fibrillation and coronary artery disease); and the use of antihypertensive, antidiabetic, lipid-lowering and antiplatelet/anticoagulant medications.

### 2.3 | Imaging acquisition

Participants' MRI scans were acquired on a 3T MRI scanner (GE Healthcare, MR750, Milwaukee, WI) equipped with a 32-channel head coil. The parameter settings for the sequences were as follows: 3D T1 BRAVO sequence, TR/TE = 8.2 ms/3.2 ms, flip angle = 12°, slice thickness = 1.2 mm, matrix size = 256 × 256, FOV = 240 × 240 mm<sup>2</sup>; Cor CUBE FLAIR sequence, TR/TE = 6,000 ms/90 ms, slice thickness = 2.0 mm, flip angle = 90°, matrix size = 256 × 256, FOV = 260 × 260 mm<sup>2</sup>; DTI sequences, TR/TE = 6,000 ms/84.4 ms, slice thickness = 4 mm, flip angle = 90°, number of diffusion directions = 25, one unweighted scan and 25 diffusion weighted scans with a *b*-value of 1,000 s/mm<sup>2</sup>, matrix size = 256 × 256, FOV = 240 × 240 mm<sup>2</sup>.

## 2.4 | WMH segmentation and diffusion MRI tractography

The WMH segmentation was performed using an automated procedure based on deep learning with U-net (Ronneberger, Fischer, & Brox, 2015). The method was described in detail in our previous study (Xia et al., 2020). Briefly, using axial slices of  $T_2$  FLAIR images as input images, the model was trained on an 11GB GTX1080ti GPU (image sources: images from the present study and a public image data set from UMC Utrecht Hospital [Kuijf et al., 2019]) and the segmentation of each image was generated automatically in 2.66 s. The  $T_2$  FLAIR images and the WMH map were registered to each subject's own diffusion images and Montreal Neurological Institute (MNI) space using FMRIB's Linear/Nonlinear Image Registration Tools (FLIRT/FNIRT), part of the FMRIB Software Library (FSL) v5.09 (Jenkinson, Beckmann, Behrens, Woolrich, & Smith, 2012). The WMH overlap frequency was obtained.

The TRActs Constrained by UnderLying Anatomy (TRACULA) tool of the FreeSurfer v6.0 image analysis suite (Yendiki et al., 2011) was used for pre-processing, tractography and group statistics analyses. TRACULA uses global probabilistic tractography with anatomical prior information of predefined WM pathways. The 18 reconstructed major WM pathways were as follows (Figure 1a): forceps major (FMA), forceps minor (FMI), corticospinal tract (CST), inferior longitudinal fasciculus (ILF), uncinate fasciculus (UNC), anterior thalamic radiation (ATR), cingulum cingulate gyrus (CCG), cingulum angular bundle (CAB), superior longitudinal fasciculus: parietal (SLFP) and temporal (SLFT). All the pathways except for the FMA and FMI were bihemispherically lateralized and labeled left and right. A threshold of 1% posterior probability of the tract was applied to create the region of interest (ROI) of each tract (Munoz Maniega et al., 2019).

## 2.5 | Distal tracts and spatial group analyses

The ROI of the WMH was dilated by 4 mm ( $x$ - $y$  plane:  $0.938 \times 4$ ,  $z$ -direction: 4) up to 12 mm and then subtracted from each WM tract

using Analysis of Functional NeuroImages (AFNI) (<https://afni.nimh.nih.gov/>) (Figure 1b). Therefore, four types of WM tract remnants (excluding areas of 0, 4, 8 and 12 mm around the WMH) were obtained and further employed to extract of the average diffusion characteristics in every participant. Specific tract remnants excluding a 12 mm region were defined as distal tracts. The spatial group-average analyses of WM tracts were also obtained by normalizing the individual WM tracts to MNI space and excluding the segments of the WM tracts' two end points that had less than 80% overlap frequency. The average diffusion characteristics along the trajectory of the pathway at different spatial positions were calculated straightforwardly according to the posterior distribution by TRACULA.

The whole-brain WMH volume measurements were expressed as the ratio of that volume to the total intracranial volume (ICV), thereby adjusting for different head sizes. The tract-specific WMH ratio was defined as the ratio of tract-specific WMH intersection volume to the corresponding tract total volume. Tract-specific WMH ratios were log-transformed because of the non-normal data distribution (Cremers et al., 2016; Seiler et al., 2018). Considering that WMH lesions are rare in the CAB in the left and right hemispheres (Figure 2), we excluded the CAB in the subsequent analysis.

## 2.6 | Cognitive function

Participants underwent neuropsychological tests in the following domains: (a) global cognitive function: Mini-Mental State Examination (MMSE) and Montreal Cognitive Assessment (MoCA); (b) memory: Auditory Verbal Learning Test (AVLT) for participants with  $\geq 6$  years of education, Huashan Object Memory Test (HOMT) for those with  $< 6$  years of education; (c) language: Common Objects Sorting Test (COST); (d) spatial construction: Stick Test; (e) attention and executive function: Trail Making Test (TMT) for participants with  $\geq 6$  years of education and the Renminbi Test for those with  $< 6$  years of education. These neuropsychological tests were translated, adapted, and normed from Western countries based on Chinese culture, and had

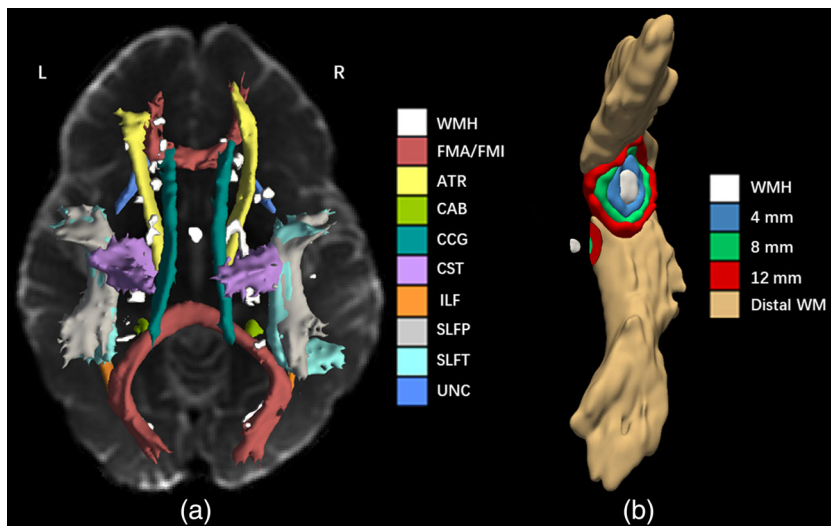
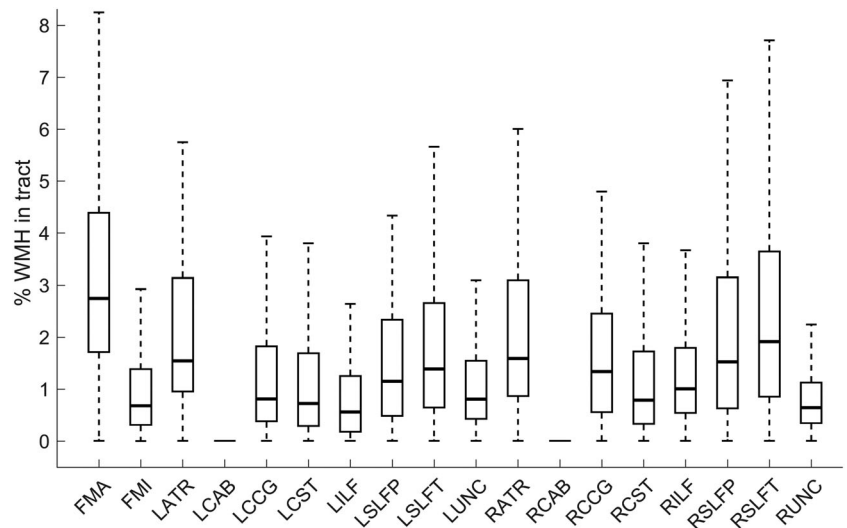


**FIGURE 1** Visualization of white matter tracts and WMH. (a) An example showing the spatial distribution of 18 major WM tracts and WMH. (b) An example of the spatial analysis contours for tracts and WMH in the CST. The surface contours were dilated by 4 mm at a time from the WMH edge. L = left; R = right; WMH = white matter hyperintensities; FMA = forceps major; FMI = forceps minor; ATR = anterior thalamic radiation; CAB = cingulum angular bundle; CCG = cingulum cingulate gyrus; CST = corticospinal tract; ILF = inferior longitudinal fasciculus; SLFP = superior longitudinal fasciculus-parietal; SLFT = superior longitudinal fasciculus-temporal; UNC = uncinate fasciculus

**FIGURE 2** Boxplots of the percentages of tract-specific WMH ratios. Boxes indicate the 25th–75th percentiles of WMH ratios, and the lines and whiskers show the median and range of WMH ratios respectively. L = left; R = right; WMH = white matter hyperintensities; FMA = forceps major; FMI = forceps minor; ATR = anterior thalamic radiation; CAB = cingulum angular bundle; CCG = cingulum cingulate gyrus; CST = corticospinal tract; ILF = inferior longitudinal fasciculus; SLFP = superior longitudinal fasciculus-parietal; SLFT = superior longitudinal fasciculus-temporal; UNC = uncinate fasciculus



been validated in previously published Chinese studies (Ding et al., 2015; Ding et al., 2016). Details of the neuropsychological tests are described in the supplementary materials. z-scores (the individual test score minus the mean test score divided by the standard deviation) were calculated for each cognitive domain.

## 2.7 | Statistical analysis

Statistical analyses were performed in R v3.61 (Team, 2019). The median (interquartile range, IQR) was used to describe the non-normally distributed continuous variables. Number (percentage) was used to describe categorical variables. The relationships between the diffusion characteristics of various remnants of WM tracts and the tract-specific WMH ratios were assessed using multivariable linear regression, adjusting for age and sex. One-way analysis of variance (ANOVA) with a post-hoc test was performed to analyze group differences. The relationships between the diffusion characteristics of distal WM tracts and cognitive function were examined by multivariable linear regression, controlling for age, sex, education and whole-brain WMH (calculated by dividing the total WMH volume by the total intracranial volume). We employed the false discovery rate (FDR) for multiple comparison correction. Both  $\beta$  coefficients and P values were two-tailed estimates, and the criterion for statistical significance was set to  $p < .05$  (Genovese, Lazar, & Nichols, 2002).

## 3 | RESULTS

The demographic, neuroimaging, and cognitive characteristics of the 174 subjects involved in the study are presented in Table 1. The percentages of tract-specific WMH ratios were distributed differently in the 18 WM tracts, but symmetrically in the left and right hemispheres (Figure 2). The FMA was most prone to the occurrence of WMH, followed by the ATR, SLFT, SLFP, CCG, and CST. However, there were almost no WMH detected in the CAB. A two-way ANOVA

was performed and there was no statistically significant interaction effect between WMH ratio and location, which indicated that the effects on MD values by the WMH are independent of the location (Table S1). More information about other diffusion characteristics (FA; axial diffusivity, AD; radial diffusivity, RD) can be found in the supplementary data.

### 3.1 | Tract-specific WMH ratios and tract diffusion characteristics

The diffusion characteristics of the FMA, FMI, bilateral ATR, CCG, CST, ILF, SLFP, SLFT, and UNC were significantly correlated with the tract-specific WMH ratios (Table 2 and Table S2). After excluding the WMH area of the tracts, the correlations of the FMA, CCG, CST, SLFP, SLFT, and UNC remained. In the FMA, CCG, SLFP, SLFT, and UNC, even when we excluded up to 12 mm around the WMH area, the correlations were consistent with those reported previously. The FMI and ILF mainly showed correlations in FA and the ATR mainly showed a correlation in MD.

For each WM tract, the 174 participants were divided into three groups (G1, G2, G3) by the tertile of the intersected WMH volume with each tract, with 58 participants in each group. Individuals in the G1 group had the smallest WMH volume and those in the G3 group had the largest WMH volume. The diffusion characteristics of distal WM tracts were plotted (Figure 3 and Figure S1). The results indicated that compared to those with a mild WMH burden, participants with a severe WMH burden tended to possess increased MD and reduced FA in distal WM tracts.

### 3.2 | WMH ratio and diffusion characteristics along tracts

The average distribution of diffusion characteristics at different positions along the trajectory of all participants' pathways in MNI space

**TABLE 1** Baseline characteristics of the study population ( $N = 174$ )

Characteristics	Median (IQR)	Number (%)
Age, years	74 (69 to 79)	
Male/female		77/97
Education, years	12 (9 to 15)	
Body mass index, (kg/m <sup>2</sup> )	23.5 (21.6 to 26.2)	
Current smoker		15 (8.6)
Hypertension		100 (57.5)
Diabetes		26 (14.9)
Hyperlipidaemia		75 (43.1)
Cardiogenic disease		24 (13.8)
Antihypertensive		99 (56.9)
Antidiabetic		30 (17.2)
Lipid lowering		34 (19.5)
Antiplatelet/ anticoagulation		27 (15.5)
Total intracranial volume, (ml)	1501.3 (1399.3 to 1596.8)	
Total WMH, (ml)	11.3 (5.0 to 12.8)	
Overall FA of tracts	0.36 (0.34 to 0.38)	
Overall MD of tracts (10 <sup>-3</sup> mm <sup>2</sup> /s)	0.86 (0.84 to 0.88)	
MoCA	25 (22 to 27)	
MMSE	29 (27 to 29)	
Memory, z score	0.00 (-0.59 to 0.78)	
Language, z score	0.21 (-0.02 to 0.44)	
Spatial construction, z score	0.00 (-0.45 to 0.44)	
Attention and executive function, z score	0.00 (-0.60 to 0.49)	

Abbreviations: FA, fractional anisotropy; IQR, interquartile range; MD, mean diffusivity; MoCA, Montreal Cognitive Assessment; MMSE, Mini-Mental State Examination; WMH, white matter hyperintensities.

was estimated, as represented in Figure 4 and Figure S2. Some of the positions on the FMA, ATR, CCG, CST, ILF, SLFP, SLFT, and UNC showed significant correlations between diffusion characteristics and tract-specific WMH ratios. The ILF did not show significant correlations with MD in any position and the RSLFT, RUNC did not show significant correlations with FA in any position. The FMI did not show correlations with FA or MD in any of the tract positions. A group difference with a two-sample *t* test (FDR corrected) was also identified between participants with and without WMH involving the tracts (Figure S3).

### 3.3 | Distal WM tracts and cognitive function

Given that tract-specific WMH were related to the impaired microstructural integrity of distal WM tracts, we further explored the

relationships between distal tract-specific diffusion characteristics and cognitive function (Table 3 and Table S3). Attention and executive function were found to be associated with the distal MD of all tracts combined ( $\beta = -0.27$ ,  $p = .004$ ) as well as the FMI ( $\beta = -0.19$ ,  $p = .018$ ), LILF ( $\beta = -0.27$ ,  $p = .002$ ), LSLFP ( $\beta = -0.24$ ,  $p = .009$ ), LSFLT ( $\beta = -0.20$ ,  $p = .015$ ), LUNC ( $\beta = -0.30$ ,  $p = .001$ ), RCCG ( $\beta = -0.20$ ,  $p = .015$ ), RSLFP ( $\beta = -0.20$ ,  $p = .015$ ), RSFLT ( $\beta = -0.22$ ,  $p = .008$ ), and RUNC ( $\beta = -0.21$ ,  $p = .015$ ) individually, after adjusting for age, sex, education and whole-brain WMH volume. There was no significant correlation between FA and cognitive function after FDR correction.

## 4 | DISCUSSION

In this community-dwelling elderly population, we found that impaired microstructural integrity of the distal WM tracts, including the FMA, ATR, CCG, CST, SLFT, SLFP, and UNC, was correlated with tract-specific WMH ratios and worse attention and executive function. The results suggested that the impact of WMH might propagate to the distal tracts outside the WMH penumbra, and consequently contribute to the impairment of attention and executive function.

Specifically, we observed that the FMA, SLFP, SLFT, and ATR WM tracts were severely vulnerable to WMH, while the CAB, FMI, and LILF WM tracts were least affected, consistent with previous results (Munoz Maniega et al., 2019). The low burden of tract-specific WMH might explain the lack of significant distal WMH effects in these tracts (Munoz Maniega et al., 2019). Another possible reason is that partial volume averaging with cerebrospinal fluid could potentially affect the variance of diffusion parameters measured in these tracts (Vos, Jones, Viergever, & Leemans, 2011).

Previous studies observed impaired microstructural integrity in the penumbra of WMH lesions, approximately 2–9 mm around the WMH itself (Maillard et al., 2014; Promjunyakul et al., 2016). Moreover, studies found a spatial gradient of diminished integrity spreading from WMH along the intersecting WM tracts (Munoz Maniega et al., 2019), suggesting that the degenerative processes of WM tracts could probably extend to the distal regions beyond penumbra through the tracts. However, it remains unclear whether this phenomenon is an effect of WMH. Our study indicated that the altered diffusion characteristics were not only observed in WMH and penumbra but also further away from the penumbra, even in the entire length of some tracts. Our study was the first to indicate that high burden of tract-specific WMH prompted deficits in distal WM tracts in a healthy elderly population, underscoring the potential disruptive effect of WMH on the distal WM tract network.

Executive function is a collection of cognitive processes (including attention) essential for advanced psychological function, which helps to adapt to a continuously changing environment (Logue & Gould, 2014). Executive function has long been considered a cognitive domain affected by vascular injuries (Gorelick et al., 2011) and was associated with conventional imaging markers of CSVD in the general population (Poels et al., 2012; Prins et al., 2005; Saczynski



**TABLE 2** Associations between MD values of WM tracts and tract-specific WMH ratios

Tract	Whole tracts		Exclude WMH		Exclude 4 mm		Exclude 8 mm		Exclude 12 mm	
	$\beta$	<i>p</i>	$\beta$	<i>p</i>	$\beta$	<i>p</i>	$\beta$	<i>p</i>	$\beta$	<i>p</i>
FMA	<b>0.35</b>	<b>&lt;.001</b>	<b>0.20</b>	<b>.007</b>	0.13	.083	<b>0.24</b>	<b>.002</b>	<b>0.29</b>	<b>&lt;.001</b>
FMI	<b>0.24</b>	<b>.002</b>	0.15	.057	0.09	.294	0.10	.221	0.14	.092
LATR	<b>0.64</b>	<b>&lt;.001</b>	<b>0.53</b>	<b>&lt;.001</b>	<b>0.48</b>	<b>&lt;.001</b>	<b>0.47</b>	<b>&lt;.001</b>	<b>0.41</b>	<b>&lt;.001</b>
LCCG	<b>0.34</b>	<b>&lt;.001</b>	<b>0.29</b>	<b>&lt;.001</b>	<b>0.28</b>	<b>&lt;.001</b>	<b>0.24</b>	<b>.003</b>	<b>0.22</b>	<b>.006</b>
LCST	<b>0.48</b>	<b>&lt;.001</b>	<b>0.42</b>	<b>&lt;.001</b>	<b>0.44</b>	<b>&lt;.001</b>	<b>0.48</b>	<b>&lt;.001</b>	<b>0.45</b>	<b>&lt;.001</b>
LILF	<b>0.22</b>	<b>.006</b>	0.07	.413	-0.10	.223	0.001	.989	0.11	.182
LSLFP	<b>0.47</b>	<b>&lt;.001</b>	<b>0.38</b>	<b>&lt;.001</b>	<b>0.34</b>	<b>&lt;.001</b>	<b>0.38</b>	<b>&lt;.001</b>	<b>0.40</b>	<b>&lt;.001</b>
LSLFT	<b>0.46</b>	<b>&lt;.001</b>	<b>0.36</b>	<b>&lt;.001</b>	<b>0.28</b>	<b>&lt;.001</b>	<b>0.31</b>	<b>&lt;.001</b>	<b>0.30</b>	<b>&lt;.001</b>
LUNC	<b>0.46</b>	<b>&lt;.001</b>	<b>0.37</b>	<b>&lt;.001</b>	<b>0.35</b>	<b>&lt;.001</b>	<b>0.34</b>	<b>&lt;.001</b>	<b>0.30</b>	<b>&lt;.001</b>
RATR	<b>0.63</b>	<b>&lt;.001</b>	<b>0.52</b>	<b>&lt;.001</b>	<b>0.51</b>	<b>&lt;.001</b>	<b>0.54</b>	<b>&lt;.001</b>	<b>0.52</b>	<b>&lt;.001</b>
RCCG	<b>0.21</b>	<b>.009</b>	0.16	.054	<b>0.18</b>	<b>.035</b>	<b>0.17</b>	<b>.042</b>	<b>0.18</b>	<b>.024</b>
RCST	<b>0.53</b>	<b>&lt;.001</b>	<b>0.46</b>	<b>&lt;.001</b>	<b>0.48</b>	<b>&lt;.001</b>	<b>0.53</b>	<b>&lt;.001</b>	<b>0.48</b>	<b>&lt;.001</b>
RILF	0.13	.082	0.003	.963	-0.04	.589	0.12	.107	<b>0.23</b>	<b>.002</b>
RSLFP	<b>0.49</b>	<b>&lt;.001</b>	<b>0.37</b>	<b>&lt;.001</b>	<b>0.28</b>	<b>&lt;.001</b>	<b>0.31</b>	<b>&lt;.001</b>	<b>0.28</b>	<b>&lt;.001</b>
RSLFT	<b>0.51</b>	<b>&lt;.001</b>	<b>0.38</b>	<b>&lt;.001</b>	<b>0.23</b>	<b>.003</b>	<b>0.23</b>	<b>.003</b>	<b>0.21</b>	<b>.006</b>
RUNC	<b>0.37</b>	<b>&lt;.001</b>	<b>0.30</b>	<b>&lt;.001</b>	<b>0.27</b>	<b>&lt;.001</b>	<b>0.26</b>	<b>&lt;.001</b>	<b>0.23</b>	<b>.004</b>

Note: Statistics of multivariable linear regression including tract-specific MD as the dependent variable and the tract-specific WMH ratio as an independent variable, adjusted for age and sex. The ROI of the WMH was dilated by 4 mm up to 12 mm and then subtracted from each WM tract. Therefore, four types of WM tract remnants (excluding areas of 0, 4, 8 and 12 mm around the WMH) were obtained. The value of  $\beta$  represents standardized regression coefficients. Bold formatting represents a significant association ( $p < .05$ , corrected by false discovery rate). Abbreviations: ATR, anterior thalamic radiation; CCG, cingulum cingulate gyrus; CST, corticospinal tract; FMA, forceps major; FMI, forceps minor; ILF, inferior longitudinal fasciculus; L, left; MD, mean diffusivity; R, right; SLFP, superior longitudinal fasciculus-parietal; SLFT, superior longitudinal fasciculus-temporal; UNC, uncinate fasciculus; WMH, white matter hyperintensities.

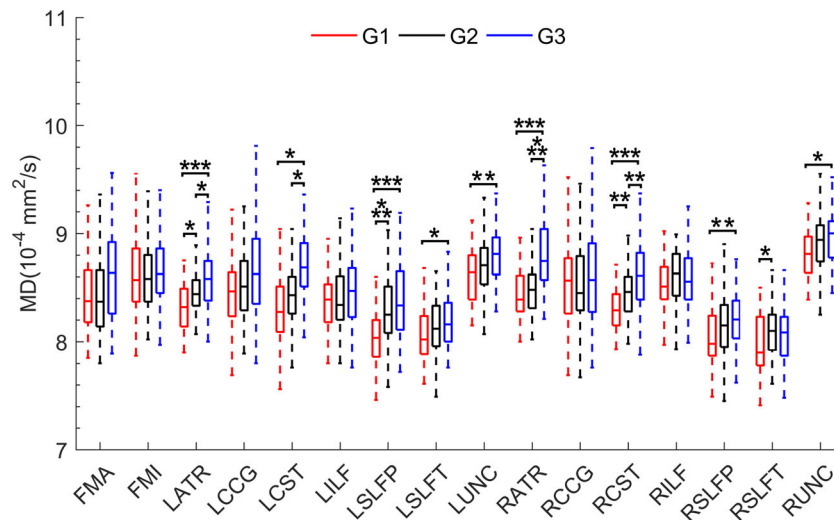


**FIGURE 3** Measurements of the MD values of the distal WM tracts. All participants ( $n = 174$ ) were divided into three groups (G1 < G2 < G3) by tertile of tract-specific WMH volume, with 58 participants in each group. Participants in the G1 group had the smallest WMH volume and those in the G3 group had the largest WMH volume. Boxes indicate the 25th–75th percentiles of MD, and the lines and whiskers show the median and range of MD respectively. One-way ANOVA analysis and post-hoc testing with Bonferroni correction were used. \* $p < .05$ . \*\* $p < .01$ . \*\*\* $p < .001$ . MD = mean diffusivity; WMH = white matter hyperintensities; L = left; R = right; FMA = forceps major; FMI = forceps minor; ATR = anterior thalamic radiation; CCG = cingulum cingulate gyrus; CST = corticospinal tract; ILF = inferior longitudinal fasciculus; SLFP = superior longitudinal fasciculus-parietal; SLFT = superior longitudinal fasciculus-temporal; UNC = uncinate fasciculus

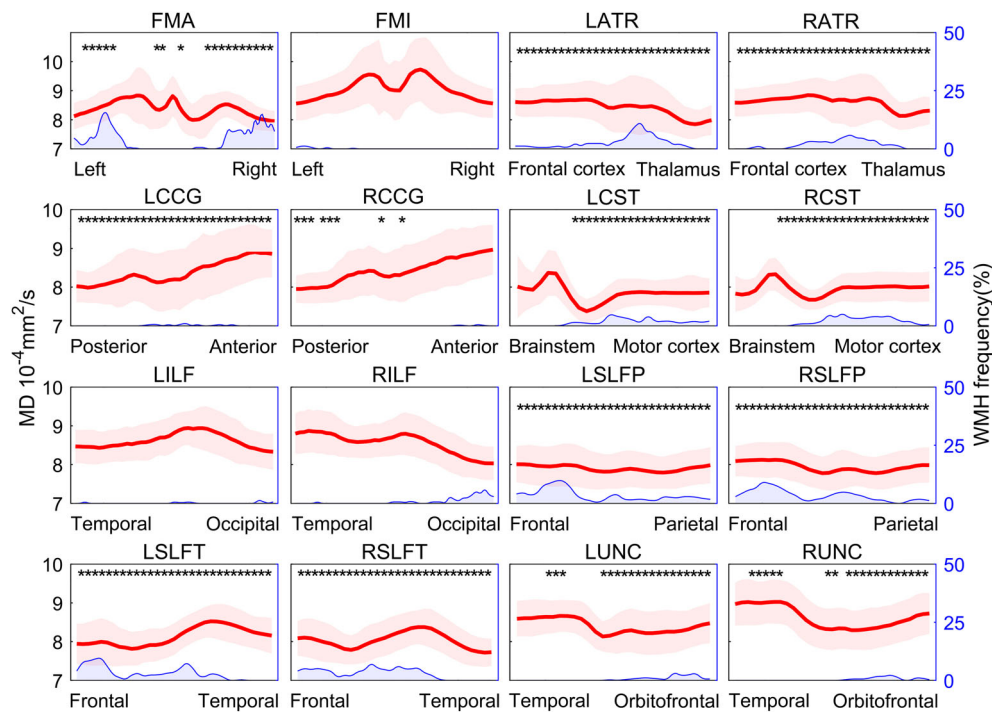


**FIGURE 4** The average MD values of all participants along each tract in MNI space. The abscissa is the spatial position along the tract, the red line represents the mean MD values and the light red interval is the standard deviation. Significant correlations ( $p < .05$ , corrected for false discovery rate) between the MD of WM tracts at each position and tract-specific WMH ratios are plotted in black \* (adjusted for age and sex). The height of the blue curve represents the percentage of WMH overlap frequency along the tracts. MD = mean diffusivity; WMH = white matter hyperintensities; L = left; R = right; FMA = forceps major; FMI = forceps minor; ATR = anterior thalamic radiation; CCG = cingulum cingulate gyrus; CST = corticospinal tract; ILF = inferior longitudinal fasciculus; SLFP = superior longitudinal fasciculus-parietal; SLFT = superior longitudinal fasciculus-temporal; UNC = uncinate fasciculus

et al., 2009). Moreover, the relationship between WM integrity within the penumbra and executive function has been previously verified in a general elderly population (Vernooij et al., 2009). The present study adds to the current knowledge that the disruption in microstructural integrity of distal tracts may also contribute to the impairment of attention and executive function, regardless of the impact of the total WMH burden. The absence of such an association in the ATR and CST could be partly explained by the distinct physiological function of these two tracts: the CST is mostly involved in motor function (Feng et al., 2015), and the ATR relays sensory and motor information from the thalamus to the cerebral cortex (Jones, 2002).

One study on patients with cerebral autosomal dominant arteriopathy with subcortical infarcts and leukoencephalopathy (CADASIL), a genetic form of CSVD, indicated that CSVD markers, such as lacunes, could induce more cortical thinning by impairing the microstructure of WM tracts connecting lacunes and the remote cortex, consequently affecting the cognitive function (Duering et al., 2012; Duering et al., 2015). Notably, our study supported the idea that the microstructural integrity of WM tracts plays a mediating role in the mechanism of vascular cognitive impairment in the general population, specifically in the domain of attention and executive function. Whether the cortex is involved in the process is a question that will need to be addressed in future research.

It has been indicated that MD is more sensitive to aging-related degeneration than other radiological markers such as FA, magnetization transfer ratio and  $T_1$  intensity (Cremers et al., 2016; Maniega et al., 2015; Reginold et al., 2015; Reginold et al., 2018), which might explain why cognition was not found to be corrected with FA. The pathology of degenerative WMH propagation is still uncertain. Some studies pointed out that an increase in MD and a decrease in FA indicated an increase in tissue water, underlying inflammation, edema (Alexander et al., 2007), vacuolization within myelin sheaths (Gouw et al., 2011) and tissue atrophy (Phillips et al., 2016). The observed deficits in the remote WM tracts might be explained by axonal loss, a Wallerian-like or retrograde degeneration (Munoz Maniega et al., 2019; Thomalla et al., 2004). The propagation of defects might also be carried out by deficits of axonal transport (Millecamps & Julien, 2013), which is necessary for the maintenance and function of axons.

The strengths of our study lie mainly in its novelty. We first verified the impact of WMH on the distal WM tracts beyond the penumbra and the role of distal WM tracts in cognitive impairment in a healthy elderly population. This finding shed light on the potential mechanism of cognitive impairment in CSVD. In addition, we conducted quantitative WMH segmentation, meticulous WM tractography, and comprehensive assessment of cognition. However, there are some limitations. First, the analysis was restricted to a relatively small sample; thus, future community studies with larger sample

**TABLE 3** Relationships between MD values of distal WM tracts and cognitive function

Tract	MoCA		MMSE		Memory		Language		Spatial		Attention and executive	
	$\beta$	<i>p</i>	$\beta$	<i>p</i>	$\beta$	<i>p</i>	$\beta$	<i>p</i>	$\beta$	<i>p</i>	$\beta$	<i>p</i>
All tracts	0.05	.501	-0.02	.804	0.01	.940	0.06	.445	0.01	.900	<b>-0.27</b>	<b>.004</b>
FMA	0.07	.286	0.06	.390	0.04	.580	0.01	.917	0.00	.985	-0.06	.423
FMI	0.05	.460	0.01	.918	0.02	.783	0.08	.311	0.00	.993	<b>-0.19</b>	<b>.018</b>
LATR	0.14	.073	0.03	.654	<b>0.20</b>	<b>.029</b>	0.11	.211	0.04	.676	-0.17	.055
LCCG	0.05	.435	-0.03	.655	0.02	.818	0.00	.963	-0.02	.817	-0.13	.088
LCST	-0.08	.242	-0.07	.268	-0.09	.252	-0.03	.675	-0.10	.189	-0.12	.111
LILF	0.01	.899	-0.06	.333	-0.07	.403	-0.02	.840	0.06	.422	<b>-0.27</b>	<b>.002</b>
LSFLP	0.04	.560	0.01	.880	0.02	.785	0.11	.186	0.02	.764	<b>-0.24</b>	<b>.009</b>
LSLFT	0.08	.297	0.01	.856	0.07	.424	0.08	.337	0.03	.683	<b>-0.20</b>	<b>.015</b>
LUNC	-0.05	.524	-0.03	.710	-0.03	.730	0.01	.941	0.03	.754	<b>-0.30</b>	<b>.001</b>
RATR	0.10	.211	-0.02	.768	0.08	.401	0.09	.348	0.09	.335	-0.18	.055
RCCG	-0.02	.740	-0.02	.746	0.08	.335	0.06	.432	-0.04	.553	<b>-0.20</b>	<b>.015</b>
RCST	0.01	.903	-0.08	.277	-0.06	.477	0.01	.910	0.08	.315	-0.07	.423
RILF	0.03	.701	-0.03	.655	-0.08	.306	0.03	.719	-0.04	.580	-0.15	.057
RSLFP	0.07	.344	0.00	.973	0.00	.998	0.14	.067	0.07	.339	<b>-0.20</b>	<b>.015</b>
RSLFT	0.06	.389	0.00	.964	0.00	.964	0.11	.128	0.08	.290	<b>-0.22</b>	<b>.008</b>
RUNC	-0.02	.815	-0.04	.589	-0.13	.128	0.02	.823	0.05	.503	<b>-0.21</b>	<b>.015</b>

Note: The MD values of distal WM tracts were acquired by: (1) removing the proximal WM tracts (within 12 mm of the WMH); and (2) calculating the MD of the remnants of the WM tracts. Adjusted for age, sex, education and the whole-brain WMH ratio. Bold formatting represents a significant association ( $p < .05$ , corrected by false discovery rate). Abbreviations: ATR, anterior thalamic radiation; CCG, cingulum cingulate gyrus; CST, corticospinal tract; FMA, forceps major; FMI, forceps minor; ILF, inferior longitudinal fasciculus; L, left; MD, mean diffusivity; R, right; SLFP, superior longitudinal fasciculus-parietal; SLFT, superior longitudinal fasciculus-temporal; UNC, uncinate fasciculus; WMH, white matter hyperintensities.

sizes are required. Second, there was a mixed effect on the overall MD values in tracts beyond the penumbra caused by WMH and various distal spatial locations. However, the current study further analyzed the correlations by controlling for the location factor. Third, our cross-sectional study mainly focused on the associations between diffusion characteristics and cognitive function. Longitudinal studies are needed in the future to assess the prognostic value of diffusion characteristics of distal tracts in predicting cognitive decline.

## 5 | CONCLUSIONS

Our results revealed an association between the microstructural integrity of distal tracts and tract-specific WMH, as well as attention and executive function. These findings suggested that microstructural changes caused by WMH might propagate further beyond the penumbra, and indicated that integrity of distal tracts may play an important role in cognitive function.

### ACKNOWLEDGMENTS

This study was funded by the National Key R&D Program of China (2016YFC1300503, 2017YFC1308201), National Natural Science Foundation of China (81971123, 81701665, 21876041), Shanghai Municipal Science and Technology Major Project (No. 2018SHZDZX01), ZJLab, and Research Center on Aging and Medicine, Fudan University.

### CONFLICT OF INTEREST

We have no financial relationships to declare and no competing interests to disclose.

### AUTHOR CONTRIBUTIONS

Yanpeng Liu, Yiwei Xia, and Xiaoxiao Wang analyzed the data and wrote the article. Yanming Wang and Du Zhang processed the data. Jiajie He and Benedictor Alexander Nguchu contributed to the writing of the article. Yi Wang, Lumeng Yang, Yiqing Wang, Yunqing Ying, Xiaoni Liang, Qianhua Zhao, Jianjun Wu, Zonghui Liang, and Ding Ding acquired and processed the data. Xing Cheng, Qiang Dong, Bensheng Qiu, and Jia-Hong Gao conceived and supervised the study and contributed to the writing of the article. All authors discussed the results and reviewed the article.

### ETHICAL STATEMENT

This study was approved by the Medical Ethics Committee of Huashan Hospital, Fudan University, Shanghai, China. Written informed consent was obtained from all participants or a legally acceptable representative.

### DATA AVAILABILITY STATEMENT

The code and data supporting the findings of this study are available from the corresponding author upon reasonable request.



## ORCID

Yanpeng Liu  <https://orcid.org/0000-0002-0089-7589>

Xiaoxiao Wang  <https://orcid.org/0000-0002-8498-7388>

Jia-Hong Gao  <https://orcid.org/0000-0002-9311-0297>

## REFERENCES

- Alexander, A. L., Lee, J. E., Lazar, M., & Field, A. S. (2007). Diffusion tensor imaging of the brain. *Neurotherapeutics*, 4(3), 316–329. <https://doi.org/10.1016/j.nurt.2007.05.011>
- Banerjee, G., Jang, H., Kim, H. J., Kim, S. T., Kim, J. S., Lee, J. H., ... Werring, D. J. (2018). Total MRI small vessel disease burden correlates with cognitive performance, cortical atrophy, and network measures in a memory clinic population. *Journal of Alzheimers Disease*, 63(4), 1485–1497. <https://doi.org/10.3233/JAD-170943>
- Black, S., Gao, F., & Bilbao, J. (2009). Understanding white matter disease: Imaging-pathological correlations in vascular cognitive impairment. *Stroke*, 40(3 Suppl), S48–S52. <https://doi.org/10.1161/STROKEAHA.108.537704>
- Cremers, L. G., de Groot, M., Hofman, A., Krestin, G. P., van der Lugt, A., Niessen, W. J., ... Ikram, M. A. (2016). Altered tract-specific white matter microstructure is related to poorer cognitive performance: The Rotterdam study. *Neurobiology of Aging*, 39, 108–117. <https://doi.org/10.1016/j.neurobiolaging.2015.11.021>
- DeCarli, C., Massaro, J., Harvey, D., Hald, J., Tullberg, M., Au, R., ... Wolf, P. A. (2005). Measures of brain morphology and infarction in the Framingham heart study: Establishing what is normal. *Neurobiology of Aging*, 26(4), 491–510. <https://doi.org/10.1016/j.neurobiolaging.2004.05.004>
- Ding, D., Zhao, Q., Guo, Q., Liang, X., Luo, J., Yu, L., ... Shanghai Aging Study. (2016). Progression and predictors of mild cognitive impairment in Chinese elderly: A prospective follow-up in the Shanghai Aging study. *Alzheimer's & Dementia (Amsterdam)*, 4, 28–36. <https://doi.org/10.1016/j.dadm.2016.03.004>
- Ding, D., Zhao, Q., Guo, Q., Meng, H., Wang, B., Luo, J., ... Hong, Z. (2015). Prevalence of mild cognitive impairment in an urban community in China: A cross-sectional analysis of the Shanghai Aging study. *Alzheimer's & Dementia*, 11(3), 300–309 e302. <https://doi.org/10.1016/j.jalz.2013.11.002>
- Ding, D., Zhao, Q., Guo, Q., Meng, H., Wang, B., Yu, P., ... Hong, Z. (2014). The Shanghai Aging study: Study design, baseline characteristics, and prevalence of dementia. *Neuroepidemiology*, 43(2), 114–122. <https://doi.org/10.1159/000366163>
- Duering, M., Righart, R., Csanadi, E., Jouvent, E., Herve, D., Chabriat, H., & Dichgans, M. (2012). Incident subcortical infarcts induce focal thinning in connected cortical regions. *Neurology*, 79(20), 2025–2028. <https://doi.org/10.1212/WNL.0b013e3182749f39>
- Duering, M., Righart, R., Wollenweber, F. A., Zietemann, V., Gesierich, B., & Dichgans, M. (2015). Acute infarcts cause focal thinning in remote cortex via degeneration of connecting fiber tracts. *Neurology*, 84(16), 1685–1692. <https://doi.org/10.1212/WNL.0000000000001502>
- Feng, W. W., Wang, J., Chhatbar, P. Y., Doughty, C., Landsittel, D., Lioutas, V. A., ... Schlaug, G. (2015). Corticospinal tract lesion load: An imaging biomarker for stroke motor outcomes. *Annals of Neurology*, 78(6), 860–870. <https://doi.org/10.1002/ana.24510>
- Genovese, C. R., Lazar, N. A., & Nichols, T. E. J. N. (2002). Thresholding of statistical maps in functional neuroimaging using the false discovery rate. 15(4), 870–878.
- Gorelick, P. B., Scuteri, A., Black, S. E., Decarli, C., Greenberg, S. M., Iadecola, C., ... Anesthesia. (2011). Vascular contributions to cognitive impairment and dementia: A statement for healthcare professionals from the American Heart Association/American Stroke Association. *Stroke*, 42(9), 2672–2713. <https://doi.org/10.1161/STR.0b013e3182299496>
- Gouw, A. A., Seewann, A., van der Flier, W. M., Barkhof, F., Rozemuller, A. M., Scheltens, P., & Geurts, J. J. (2011). Heterogeneity of small vessel disease: A systematic review of MRI and histopathology correlations. *Journal of Neurology, Neurosurgery, and Psychiatry*, 82(2), 126–135. <https://doi.org/10.1136/jnnp.2009.204685>
- Jenkinson, M., Beckmann, C. F., Behrens, T. E., Woolrich, M. W., & Smith, S. M. (2012). FSL. *NeuroImage*, 62(2), 782–790. <https://doi.org/10.1016/j.neuroimage.2011.09.015>
- Jones, E. G. (2002). Thalamic circuitry and thalamocortical synchrony. *Philosophical Transactions of the Royal Society of London. Series B, Biological Sciences*, 357(1428), 1659–1673. <https://doi.org/10.1098/rstb.2002.1168>
- Kuijf, H. J., Biesbroek, J. M., de Bresser, J., Heinen, R., Andermatt, S., Bento, M., ... Biessels, G. J. (2019). Standardized assessment of automatic segmentation of white matter hyperintensities and results of the WMH segmentation challenge. *IEEE Transactions on Medical Imaging*, 38(11), 2556–2568. <https://doi.org/10.1109/Tmi.2019.2905770>
- Logue, S. F., & Gould, T. J. (2014). The neural and genetic basis of executive function: Attention, cognitive flexibility, and response inhibition. *Pharmacology Biochemistry and Behavior*, 123, 45–54. <https://doi.org/10.1016/j.pbb.2013.08.007>
- Maillard, P., Fletcher, E., Lockhart, S. N., Roach, A. E., Reed, B., Mungas, D., ... Carmichael, O. T. (2014). White matter hyperintensities and their penumbra lie along a continuum of injury in the Aging brain. *Stroke*, 45(6), 1721. <https://doi.org/10.1161/Strokeaha.113.004084>
- Maniega, S. M., Hernandez, M. C. V., Clayden, J. D., Royle, N. A., Murray, C., Morris, Z., ... Wardlaw, J. M. (2015). White matter hyperintensities and normal-appearing white matter integrity in the aging brain. *Neurobiology of Aging*, 36(2), 909–918. <https://doi.org/10.1016/j.neurobiolaging.2014.07.048>
- Millecamps, S., & Julien, J. P. (2013). Axonal transport deficits and neurodegenerative diseases. *Nature Reviews Neuroscience*, 14(3), 161–176. <https://doi.org/10.1038/nrn3380>
- Munoz Maniega, S., Meijboom, R., Chappell, F. M., Valdes Hernandez, M. D. C., Starr, J. M., Bastin, M. E., ... Wardlaw, J. M. (2019). Spatial gradient of microstructural changes in normal-appearing white matter in tracts affected by white matter hyperintensities in older age. *Frontiers in Neurology*, 10, 784. <https://doi.org/10.3389/fneur.2019.00784>
- Phillips, O. R., Joshi, S. H., Piras, F., Orfei, M. D., Iorio, M., Narr, K. L., ... Di Paola, M. (2016). The superficial white matter in Alzheimer's disease. *Human Brain Mapping*, 37(4), 1321–1334. <https://doi.org/10.1002/hbm.23105>
- Poels, M. M., Ikram, M. A., van der Lugt, A., Hofman, A., Niessen, W. J., Krestin, G. P., ... Vernooij, M. W. (2012). Cerebral microbleeds are associated with worse cognitive function: The Rotterdam scan study. *Neurology*, 78(5), 326–333. <https://doi.org/10.1212/WNL.0b013e3182452928>
- Prins, N. D., van Dijk, E. J., den Heijer, T., Vermeer, S. E., Jolles, J., Koudstaal, P. J., ... Breteler, M. M. (2005). Cerebral small-vessel disease and decline in information processing speed, executive function and memory. *Brain*, 128(Pt 9), 2034–2041. <https://doi.org/10.1093/brain/awh553>
- Promjunyakul, N. O., Lahna, D. L., Kaye, J. A., Dodge, H. H., Erten-Lyons, D., Rooney, W. D., & Silbert, L. C. (2016). Comparison of cerebral blood flow and structural penumbras in relation to white matter hyperintensities: A multi-modal magnetic resonance imaging study. *Journal of Cerebral Blood Flow and Metabolism*, 36(9), 1528–1536. <https://doi.org/10.1177/0271678X16651268>
- Reginold, W., Itorralba, J., Luedke, A. C., Fernandez-Ruiz, J., Reginold, J., Islam, O., & Garcia, A. (2016). Tractography at 3T MRI of corpus callosum tracts crossing white matter hyperintensities. *American Journal*

- of *Neuroradiology*, 37(9), 1617–1622. <https://doi.org/10.3174/ajnr.A4788>
- Reginold, W., Luedke, A. C., Tam, A., Itorralba, J., Fernandez-Ruiz, J., Reginold, J., ... Garcia, A. (2015). Cognitive function and 3-tesla magnetic resonance imaging tractography of white matter hyperintensities in elderly persons. *Dementia and Geriatric Cognitive Disorders Extra*, 5(3), 387–394. <https://doi.org/10.1159/000439045>
- Reginold, W., Sam, K., Poulblanc, J., Fisher, J., Crawley, A., & Mikulis, D. J. (2018). Impact of white matter hyperintensities on surrounding white matter tracts. *Neuroradiology*, 60(9), 933–944. <https://doi.org/10.1007/s00234-018-2053-x>
- Ronneberger, O., Fischer, P., & Brox, T. (2015). U-net: Convolutional networks for biomedical image segmentation. Paper presented at the *International conference on medical image computing and computer-assisted intervention*.
- Saczynski, J. S., Sigurdsson, S., Jonsdottir, M. K., Eiriksdottir, G., Jonsson, P. V., Garcia, M. E., ... Launer, L. J. (2009). Cerebral infarcts and cognitive performance: Importance of location and number of infarcts. *Stroke*, 40(3), 677–682. <https://doi.org/10.1161/STROKEAHA.108.530212>
- Schilling, K. G., Daducci, A., Maier-Hein, K., Poupon, C., Houde, J. C., Nath, V., ... Descoteaux, M. (2019). Challenges in diffusion MRI tractography – lessons learned from international benchmark competitions. *Magnetic Resonance Imaging*, 57, 194–209. <https://doi.org/10.1016/j.mri.2018.11.014>
- Seiler, S., Fletcher, E., Hassan-Ali, K., Weinstein, M., Beiser, A., Himali, J. J., ... Maillard, P. (2018). Cerebral tract integrity relates to white matter hyperintensities, cortex volume, and cognition. *Neurobiology of Aging*, 72, 14–22. <https://doi.org/10.1016/j.neurobiolaging.2018.08.005>
- Team, R. C. (2019). *R: A language and environment for statistical computing*. Vienna, Austria: R Foundation for Statistical Computing Retrieved from <https://www.R-project.org/>
- Thomalla, G., Glauche, V., Koch, M. A., Beaulieu, C., Weiller, C., & Rother, J. (2004). Diffusion tensor imaging detects early Wallerian degeneration of the pyramidal tract after ischemic stroke. *NeuroImage*, 22(4), 1767–1774. <https://doi.org/10.1016/j.neuroimage.2004.03.041>
- Vernooij, M. W., Ikram, M. A., Vrooman, H. A., Wielopolski, P. A., Krestin, G. P., Hofman, A., ... Breteler, M. M. (2009). White matter microstructural integrity and cognitive function in a general elderly population. *Archives of General Psychiatry*, 66(5), 545–553. <https://doi.org/10.1001/archgenpsychiatry.2009.5>
- Vos, S. B., Jones, D. K., Viergever, M. A., & Leemans, A. (2011). Partial volume effect as a hidden covariate in DTI analyses. *NeuroImage*, 55(4), 1566–1576. <https://doi.org/10.1016/j.neuroimage.2011.01.048>
- Wardlaw, J. M., Smith, C., & Dichgans, M. (2019). Small vessel disease: Mechanisms and clinical implications. *Lancet Neurology*, 18(7), 684–696. [https://doi.org/10.1016/S1474-4422\(19\)30079-1](https://doi.org/10.1016/S1474-4422(19)30079-1)
- Wardlaw, J. M., Smith, E. E., Biessels, G. J., Cordonnier, C., Fazekas, F., Frayne, R., ... Changes, S. R. V. (2013). Neuroimaging standards for research into small vessel disease and its contribution to ageing and neurodegeneration. *Lancet Neurology*, 12(8), 822–838. [https://doi.org/10.1016/S1474-4422\(13\)70124-8](https://doi.org/10.1016/S1474-4422(13)70124-8)
- Xia, Y. W., Shen, Y., Wang, Y., Yang, L. M., Wang, Y. Q., Li, Y., ... Dong, Q. (2020). White matter hyperintensities associated with progression of cerebral small vessel disease: A 7-year Chinese urban community study. *Aging-US*, 12(9), 8506–8522. <https://doi.org/10.18632/aging.103154>
- Yendiki, A., Panneck, P., Srinivasan, P., Stevens, A., Zollei, L., Augustinack, J., ... Fischl, B. (2011). Automated probabilistic reconstruction of white-matter pathways in health and disease using an atlas of the underlying anatomy. *Frontiers in Neuroinformatics*, 5, 23. <https://doi.org/10.3389/fninf.2011.00023>

## SUPPORTING INFORMATION

Additional supporting information may be found online in the Supporting Information section at the end of this article.

**How to cite this article:** Liu Y, Xia Y, Wang X, et al. White matter hyperintensities induce distal deficits in the connected fibers. *Hum Brain Mapp*. 2021;42:1910–1919. <https://doi.org/10.1002/hbm.25338>